

Mechanistic Insight into the Fluorescence Activity of Forensic Fingerprinting Reagents

L. M. Hunnisett*,^{1, a)} P. F. Kelly,¹ S. Bleay,² F. Plasser,¹ R. King,³ B. McMurchie,³ and P. Goddard¹

¹⁾Department of Chemistry, Loughborough University, Epinal Way, Loughborough, LE11 3TU, UK^{b)}

²⁾School of Applied Sciences, London South Bank University, 103 Borough Road, London SE1 0AA, UK

³⁾Foster and Freeman LTD., Vale Park, Evesham, Wrexham, WR11 1TD, UK

(Dated: 5 March 2021)

Fingerprint detection is still the primary investigative technique for deciphering criminal inquiries and identifying individuals. The main forensic fingerprinting reagents (FFRs) **currently in use can require multiple treatment steps to produce fingerprints of sufficient quality**. Therefore, the development of new, more effective FFRs that **require minimal chemical treatment** is of great interest in forensic chemistry. In this work, prudently crafted DFT and TDDFT calculations are utilised to derive mechanistic insight into the optical activity of the non-fluorescent product of ninhydrin, diketohydrindylidenediketohydrindamine (DYDA), and fluorescent product of DFO (1,8-Diazafluoren-9-one). We investigate various protonation sites **to gain an understanding of isomeric preference in the solid-state material**. A relaxed scan of a single torsion angle rotation in the S_1 minimised geometry of the O-protonated DYDA isomer suggests a conical intersection upon ~ 10 rotation. We show that the absence of a rigid hydrogen-bonded network in the crystal structure of DYDA supports the hypothesis of torsion rotation which leads to de-excitation to occur readily. Conversely, for the fluorescent DFO product, our calculations support an avoided crossing suggestive of a non-radiative mechanism when the torsion angle is rotated by about ~ 100 . This mechanistic insight concurs with experimental observations of fluorescence activity in DFO, **and may aid the photophysical understanding of poorly visualised fingerprints due to weak fluorescence**. We show that, identifying suggestive avoided crossings via the method described here can be used to initialise thoughts towards computational design of FFRs.

I. INTRODUCTION

The use of fingerprint development for forensic detection is a powerful investigative tool, providing robust evidence leading to the identification of individuals of interest in crime scene investigations.¹ The application of forensic fingerprinting reagents (FFRs) to the development of latent fingermarks on porous surfaces is a commonly encountered process in forensic chemistry and is of continuous interest to advance alongside the continued evolution of chemical analysis techniques. With the use of computational chemistry methods emerging as an effective tool in informing development processes in chemical sciences,²⁻⁴ it is of interest to apply such methods to forensic chemistry. The subsequent work, reported here, is aimed at informing the design process of fluorescent-inducing amino-acid FFRs, and investigates the structural and electronic properties of the chemical products formed when developing fingerprints using 1,8-diazafluoren-9-one (DFO), a fluorescent FFR, and 2,2-dihydroxyindane-1,3-dione (ninhydrin), a non-fluorescent FFR (fig. 1).

Ninhydrin and DFO are commonly utilised as FFRs for the development of latent fingerprints on porous surfaces.⁵ Both reagents react with trace amounts of amino acids within fingerprint residue to form chromophoric chemical products.^{6,7} Only that of DFO exhibits fluorescence emission upon light

FIG. 1. The chemical structures of ninhydrin (*left*) and DFO (*right*).

excitation during fingerprint visualisation, while the ninhydrin product requires the addition of $ZnCl_2$ to produce a fluorescent product.⁸ Fluorescence is a desirable property for developed fingerprints to maximise the observed contrast between the fingerprint pattern and background surface, increasing the detail observed and detected.¹ To obtain this in a single reaction step provides forensic investigators with a more efficient fingerprinting method and reduces the required chemical resources over those requiring additional reagents or treatments.

Ninhydrin, when reacted with amino acids, forms 'Ruhemann's Purple' (**1**), as shown in fig. 2, though it is the protonated form, diketohydrindylidenediketohydrindamine (DYDA) that is responsible for the observed characteristics of the developed fingerprint.^{9,10} This structure was elucidated

^{a)}Also at Cambridge Crystallographic Data Centre, 12 Union Road, Cambridge, CB2 1EZ, England

^{b)}Electronic mail: Authors to whom correspondence should be addressed: lhunnisett@ccdc.cam.ac.uk and p.goddard@lboro.ac.uk

This is the author's peer reviewed, accepted manuscript. However, the online version of record will be different from this version once it has been copyedited and typeset.
PLEASE CITE THIS ARTICLE AS DOI:10.1063/1.50040555

FIG. 2. The proposed chemical structures of the products from the reaction of ninhydrin with amino acids, Ruhemann's purple (**1**) and DYDA (**2-4**), and the proposed isomers of the product of the reaction of DFO with amino acids (**5** and **6**).

through X-ray crystallography and ^1H NMR, though there are inconsistencies in the reported site of protonation resulting in possible isomers, **2** and **3** respectively. Furthermore, a computational study employing a semi-empirical method suggested that **4** showed closest agreement between the calculated absorption properties and that observed experimentally (a single absorption peak with λ_{max} of 485 nm).^{9,11}

DFO reacts with amino acids during fingerprint development to form a fluorescent product, reported to exhibit excitation with λ_{max} at 470 nm and emission λ_{max} at ~ 570 nm.⁷ The crystal structure of the DFO product was determined to be **5**, though it was proposed that the proton is mobile with respect to the remaining nitrogens within the structure, resulting in **6**.¹²

Currently, the most efficient fluorescence-inducing FFR recommended for fingerprint development is 1,2-Indanedione, reported to produce brighter fluorescent fingerprints than DFO.¹³⁻¹⁵ However, structure elucidation of the fluorescent product reported in the literature has yielded conflicting results leading to no conclusive solid-state structure.^{16,17} This work has therefore focused on the DFO product to investigate fluorescent properties.

Previous attempts at the development of new, more effective FFRs have predominantly been based on experimental synthesis with little success reported.¹⁸⁻²¹ Computational studies investigating energetics of the amino acid reaction, and wavelength and oscillator strength of absorption for DYDA analogues also resulted in no new developments, highlighting the need for an alternative computational approach.²²⁻²⁴

The mechanism of fluorescence is extremely challenging to incorporate into computational design processes due to the complex relationship between structure and observed prop-

FIG. 3. An illustration of the ground (S_0) and excited (S_1) states of a chemical system demonstrating possible features and resultant relaxation mechanisms during a single excitation event, where (ii) and (iv) show absorption and excitation, and (i) and (iii) represent features indicative of a non-radiative mechanism, conical intersection and avoided crossing respectively.

erties in solid state materials. However, investigation into the potential energy surface (PES) of non-luminescent compounds can reveal non-radiative processes such as those illustrated by fig. 3.^{25,26} It is the topologies of the S_0 and lowest excited state PES that fundamentally determines the observed fluorescence activity, or inactivity, of a chemical system. A conical intersection (CI), represented by (i) in fig. 3, is a dominant non-radiative feature in non-fluorescent materials, playing a major role in the de-excitation process.²⁷ This has been demonstrated for solid-state materials using *ab initio* calculations.^{28,29}

In this work we examine the calculated absorption and emission properties of the proposed isomeric structures **2-4** (DYDA), and **5** and **6** (DFO product) to indicate the most likely structures responsible for the reported experimentally observed optical properties. The S_0 and S_1 state PES representing torsion angle rotations in those identified most likely are also explored to rationalise the observed non-fluorescent and fluorescent properties of the DYDA and the DFO product structures.

II. COMPUTATIONAL DETAILS

S_0 and S_1 minima of all molecules studied were optimised with DFT and TDDFT, respectively, using the CAM-B3LYP functional³⁰⁻³² and 6-31G(d) basis set.³³⁻³⁵ Here, the range-separated functional CAM-B3LYP was employed in order to avoid spurious charge transfer excited states³⁶ between the two units of the molecules studied, which was observed in

TABLE I. Experimentally-determined and computed photophysical properties of the materials investigated; absorption wavelength (λ_{abs}) of the lowest three transitions, emission wavelength (λ_{em}), corresponding oscillator strength (f), and character assignment for emission.

	$\lambda_{\text{abs}}^{\text{a}}$ (nm)	$\lambda_{\text{em}}^{\text{a}}$ (nm)	$\lambda_{\text{abs}}^{\text{b}}$ (nm)	$f_{\text{abs}}^{\text{b}}$	$\lambda_{\text{em}}^{\text{b}}$ (nm)	f_{em}^{b}	character ^c
1	579, 410	-	515.36, 410.9, 403.1	0.2314, 0.0131, 0.0143	- [†]	- [†]	- [†]
2			414.3, 399.4, 378.2	0.0001, 0.4262, 0.5531	921.5	0	$n \rightarrow \pi^*$
3	485	-	476.3, 378.6, 331.9	0.0001, 0, 0.0254	569.6	0	$n \rightarrow \pi^*$
4a			489.9, 396.0, 371.4	0.1092, 0.1661, 0.0006	625.2	0.0799	$n \rightarrow \pi^*$
4b			478.9, 417.2, 374.0	0.0005, 0.6086, 0	667.5	0.0916	$n \rightarrow \pi^*$
5	470	570	452.7, 395.1, 394.0	0.3567, 0.0004, 0.4564	555.9	0.0566	$\pi \rightarrow \pi^*$
6			471.9, 360.3, 359.2	0.8994, 0.001, 0.0008	562.8	0.6208	$\pi \rightarrow \pi^*$

^a Experimentally determined. ^b Computed at the CAM-B3LYP/6-31G(d) level of theory *in vacuo*. ^c character assigned from generated natural transition orbitals. [†] Optimisations failed to converge.

preliminary calculations. No dispersion correction was used as dispersion is expected to have only a minor influence on these planar structures. Calculations were performed in vacuum as there is no straightforward way of including the solid-state environment of interest. The steepest decent search algorithm was initially employed for S_1 state optimisations, followed by the GEDIIS algorithm for the relaxed scan of torsion angles.³⁷ All calculations were carried out in the gas phase using the Gaussian09 program.³⁸ Natural transition orbitals³⁹ were visualised using the GaussView 5.0 software.⁴⁰ The crystal structure of DYDA was obtained from the Cambridge Structural Database and analysed using the Mercury visualisation program.^{41,42}

III. RESULTS AND DISCUSSION

A. Calculation of absorption and emission wavelengths

The absorption wavelength (λ_{abs}) of DYDA, the non-fluorescent product of the reaction of ninhydrin with amino acids, has been experimentally determined at 485 nm.⁹ There have been conflicting reports of structure elucidation resulting in three possible structural isomers (**2-4**), differing by the site of protonation.⁹⁻¹¹ Considering conformational change, **4** may exhibit two conformational isomers, **4a** or **4b** (figure 4).

The measured absorption wavelength (λ_{abs}) and emission wavelength (λ_{em}) of the materials investigated are reported in table I alongside the calculated λ_{abs} of the three lowest energy singlet transitions, calculated λ_{em} , and corresponding oscillator strengths (f). To calculate the emission properties for each structure, an S_1 energy minimisation was initiated from the S_0 minimised geometry. The calculated λ_{abs} of **1** suggests absorption of 515.36 nm with high f (0.2314) while two dark states are present at 410.9 nm and 403.1 nm. The computed maximum is somewhat blueshifted compared to the experimental peak at 579 nm. This shift of about 0.25 eV may be attributed in part to the shift between vertical excitation and band maximum for simulated spectra⁴³ and generally lies within the expected accuracy of TDDFT. The properties of the S_0 - S_1 transition in the DYDA isomers suggest that **4a**, the O-protonated isomer shows the closest agreement with the experimental absorption wavelength of 485 nm, with a calculated λ_{abs} of 489.9 nm and f of 0.1092. The first excited states for isomers **3** and **4b** are in a similar energy range, but the calculated oscillator strengths show that these are dark states, which are probably not observed in the spectrum. **2** and **4b** feature bright states at 399 nm and 417 nm, significantly blue-shifted when compared to the experimental absorption maximum. Despite **4a** showing the closest agreement with experimental absorption, the experimental λ_{abs} was measured in CHCl_3 and so the conclusion of which isomer is most likely to occur based on the comparison of λ_{abs} is made with caution due to the *in vacuo* environment of the simulations. The calculated λ_{em} of DYDA isomers **3** - **4b** show zero f for the lowest energy transition of **2** and **3**, and weak f (0.0799 and 0.0916) for **4a** and **4b** respectively. The assigned character of the natural transition orbitals (NTOs) of S_1 minimised ge-

FIG. 4. The two possible conformers of **4**, the O-protonated isomer of DYDA, where (a) has no hydrogen bonding possibility and (b) a rearrangement accommodating hydrogen bonding.

This is the author's peer reviewed, accepted manuscript. However, the online version of record will be different from this version once it has been copyedited and typeset.
PLEASE CITE THIS ARTICLE AS DOI:10.1063/1.50040555

FIG. 5. Visualisation of the crystal packing in the previously reported X-ray crystal structure of DYDA.

ometries also suggests $n \rightarrow \pi^*$ character. The non-radiative hole-electron NTO pair calculated for isomer **2** (fig. 6 supports the non-fluorescent behaviour of the solid-state structure of DYDA. Both of the observed characteristics of emission for the DYDA isomers are suggestive of non-radiative behaviour for all possible isomers.

To gain insight into the relative stability of each isomer, relative energies of the S_0 and S_1 optimised structures under investigation have been calculated and are shown in table II. Interestingly, **4a** is shown to be the least stable (+34.09 kJmol⁻¹) despite showing the closest match with experiment, while **2**, the isomer representing the X-ray crystal structure, is the most stable.

TABLE II. Relative energies (ΔE) of the S_0 minimised geometries, and S_1 energy of the S_1 minimised geometries, investigated with respect to the most stable in each electronic state, calculated at the CAM-B3LYP/6-31G(d) level of theory.

	S_0 ΔE (kJmol ⁻¹)	S_1 ΔE (kJmol ⁻¹)
2	0.00	1.79
3	20.97	24.53
4a	34.09	70.49
4b	12.31	0.00
5	0.00	6.81
6	0.75	0.00

The calculated ΔE for the S_1 minimised geometries of **2-4b** (table II) suggest that **2** and **4b** are most stable with similar energies (1.79 kJmol⁻¹ difference), while the instability of **4a** with respect to the remaining isomers (+70.49 kJmol⁻¹) is further increased in comparison to that in the S_0 state. The difference in isomer stability between S_0 and S_1 states suggests that isomerisation may be favoured in the excited state between

2 (N-protonated) and **4b** (O-protonated). Visualisation of the X-ray crystal structure (fig. 5), indicative of the likely stabilising intermolecular interactions present within the solid-state fingerprint material, displays intermolecular hydrogen bonding between an N-H proton, and carbonyl-O simultaneously across two DYDA molecules, resulting in dimers throughout the structure. This interaction indicates a possibility of concurrent intermolecular proton transfer to occur, representing isomerisation between structures **2** and **4b**.

The calculated properties of DFO product isomers **5** and **6**, shown in table I, both show non-zero f for the lowest energy absorption transitions (0.3567 and 0.8994). Comparison of the corresponding λ_{abs} (452.7 nm for **5** and 471.9 nm for **6**) indicates that **6** matches more closely with experiment. The calculated λ_{em} of **6** (562.8 nm) also shows closest agreement with the experimental λ_{em} of 570 nm in comparison to **5** (555.9 nm). The corresponding f also indicates that this transition has near-zero possibility in **5**, whereas **6** has a comparatively high f . $\pi \rightarrow \pi^*$ character is assigned to both S_1 minimised structures, indicated by hole-electron NTOs. In fig. 6 the hole-electron NTOs for structures **2** and **6** are shown to support character assignments. More details can be found in the supplementary information. Calculated ΔE of the S_0 -minimised structures of **5** and **6** suggest their stabilities are similar (0.75 kJmol⁻¹ difference), whereas **6** is 6.81 kJmol⁻¹ more stable for the S_1 minimised structures. Both the calculated transition properties and relative stabilities suggest that **6** is more likely to be representative of the structure displaying the observed absorption and emission during fingerprint visualisation. It should be noted, that the crystal structure reported was a hydrated structure, and is most likely not representative of that present in the developed fingerprint as the DFO fingerprint development process involves thorough drying of the

FIG. 6. Natural transition orbitals (NTOs) of the hole-electron pairs for the S_1 minimised geometries of **2** and **6**.

FIG. 7. Relaxed S_1 torsion angle scans of DYDA isomer 4a (*left*), and the DFO product isomer 6 (*right*). Geometries shown are representative of the solid points.

fingerprint sample in an oven prior to visualisation.

To gain further insight into the underlying mechanisms of fluorescence activity in both DYDA and DFO, it is of interest to explore the PES topologies to identify the presence of non-radiative processes in that of DYDA to rationalise the non-fluorescent properties observed beyond that reported already here.

B. Investigation of potential energy surface topology

Non-radiative processes can be identified from the investigation of the ground and excited state PESs representing mechanisms or structural change exhibited by the material.^{25,26,28,29} In this present work the investigation of the S_0 and S_1 PESs representing a central C-C-N-C torsion angle rotation of **4a** and **5** are reported in the excited state. Isomer **4a** was chosen for this investigation due to a closer resem-

blance than **4b** of the geometry exhibited in the X-ray crystal structure, and will therefore give a more relevant insight into the hypothesised isomerisation between **2** and **4b** suggested by the calculated S_0 and S_1 energetics.

A relaxed scan of the C=N-C-C torsion angle of **4a** and **5** (fig. 7) was initiated from the optimised S_1 geometries, and carried out in 10 increments for **4a** and 20 increments for **5**. Smaller increments were explored for **4a** as an initial 20 scan did not provide a clear topology, prompting a more detailed investigation. The adjacent C-C=N-C torsion angle was fixed at the angle exhibited in the optimised S_1 geometry (17.5 for **4a**, -0.2 for **5**).

The plotted energies of the S_1 minimised geometry, and the relative S_0 energy indicated by the S_0 - S_1 transition with respect to the varied torsion angle at each step in the scan are displayed in fig. 7. The resultant PESs, plotted relative to the most stable S_0 geometry in each case, reveals contrasting topologies for **4a** and **5**. Of particular significance is the CI suggested by the PES of **4a** occurring at a torsion angle of -62.3, a 10 rotation from the unrestricted S_1 minimised geometry, which is lower in energy. The existence of this CI is further evidenced by the suggestive relative S_0 and S_1 PES topologies between -72.3 and -112.3. The S_1 PES also indicates a more stable geometry at -82.3 suggesting the S_1 minimised geometry at -52.3 is a local minimum, though closer in conformation to the S_0 minimised geometry.

The relative S_0 and S_1 PES topologies of the relaxed torsion angle scan of **5** resembles an avoided crossing (described previously in fig. 3), suggesting a lower energy S_1 minimised structure at 99.8. The relative S_0 energy is higher for this geometry compared to that at -0.2 (the unrestricted S_1 minimised geometry). In contrast to the relaxed torsion scan of **4a**, there is no evidence of a CI in that of **5**. The discussed avoided crossing suggests the existence of a nearby non-radiative mechanism when the torsion angle is rotated to 99.8, though considering the solid-state nature of the fingerprint material, this conformational change is assumed to be hindered by intermolecular bonding networks.

Visualisation of the reported crystal structure of DYDA (fig. 5) displays hydrogen bonded dimers, exhibiting two simultaneous N-H...O interactions.¹⁰ Though the structure indicates the existence of form **2**, we propose that intermolecular proton transfer occurs in the solid state material to form **4a**, explaining the agreement of the calculated λ_{abs} with experiment for the latter. Since the crystal packing does not exhibit long hydrogen-bonded networks, but dimer units, it is hypothesised that this less rigid structure allows for rotation of the torsion angle that has been investigated here, likely to occur through vibrational modes. The reported crystal structure of the DFO product resembles isomer **5**, though in hydrated form.¹² Since the suggested fingerprint development process using DFO requires heating of the sample to dry thoroughly prior to visualisation,¹ it is assumed that the crystal packing is unlikely to represent that present in the visualised fingerprint material. Further work is proposed to investigate computationally the geometries and hydrogen bonding networks of **4a** and **5** in the solid form to provide further insight into the proposed mechanistic processes.

IV. CONCLUSIONS

In this work we have applied DFT and TDDFT in the investigation of the isomeric structures of the forensic fingerprinting reagents products of ninhydrin and DFO, and provide mechanistic insight into their fluorescence activity based on conformational change.

The most likely isomeric forms of the non-fluorescent ninhydrin product, DYDA, and the fluorescent DFO product that exhibit the previously reported observed optical properties following fingerprint development have been discussed. The calculation of absorption properties using DFT and TDDFT indicate that **4a** (λ_{abs} of 489.9 nm and f of 0.1092) shows highest agreement with the experimentally reported λ_{abs} (485 nm). Despite the reported crystal structure of DYDA indicating protonation at the central N atom (form **2**), our calculated λ_{abs} (471.9 nm) and weak oscillator strength (0.0001) suggests protonation at the carbonyl (C=O) to be more likely. Calculated ΔE suggests **2** (N-protonated) and **4b** (O-protonated) are most stable in S_0 and S_1 states respectively, suggesting a proton-transfer isomerisation process may be favourable. The interactions present in the X-ray crystal structure suggest this could occur intermolecularly via isomer **4a**. In the DFO case, both the calculated λ_{abs} and λ_{em} of **6** (471.9 nm and 562.8 nm respectively) show close agreement with the reported experimental values of the DFO product (470 nm and 570 nm). Calculated energetics suggest similar S_0 stabilities for **5** and **6**, with the latter being 6.81 kJmol⁻¹ more stable in the excited state.

A relaxed S_1 scan representing a torsion angle rotation in **4a** and **5** revealed contrasting topologies of the plotted PESs. Initiated from the S_1 minimised geometries, a suggestive conical intersection is observed upon 10 rotation from the S_1 minimised geometry in **4a**. A 10 torsion rotation is considered feasible in the solid form of **4a**, hypothesised to be exhibited by vibrational modes. It is proposed that isomerisation occurs between forms **2** and **4a** via a simultaneous intermolecular proton transfer across dimers in the solid-state, explaining the observation of form **2** in the reported crystal structure. On the contrary, for the DFO product, an avoided crossing upon a 100 torsion angle rotation is observed in **5** with no indication of a potential conical intersection. This mechanistic insight from simulation reflects the strong fluorescence exhibited by the DFO product experimentally. Further solid-state calculations are suggested to confirm the nature of the crystal packing of **4a** and **5**, and to gain insight into the relative energetics of the possible isomeric forms to further evidence the mechanistic process proposed here. We should note that in a developed fingerprint sample, there would be other materials present (from the fingerprint residue/sweat, impurities, and the surface it is developed on). To include the interactions with these components would be useful, but it is impossible to know what exactly they would be considering the impurities such as dirt, cosmetic product and such like that could be present. Furthermore, fingerprint residue varies from person-to-person, day-to-day, and contains both hydrophilic and hydrophobic components. Interactions with water could be modelled but could be misleading and therefore has not

been included in this study.

The results presented here have demonstrated the successful application of TDDFT to calculate the absorption and emission properties of the products formed from well-known FFRs and suggests strong correlation between the modelled S_1 electronic properties and the observed fluorescence activity. The ability to describe the accessibility of non-radiative processes in the materials reported here offers the first step towards the design of new fluorescence-inducing reagents for fingerprint development from first principles.

V. DATA AVAILABILITY STATEMENT

The data that supports the findings of this study are available within the article and its supplementary material and can also be requested from the corresponding authors.

VI. SUPPLEMENTARY INFORMATION

In the supplementary information, we supply the computed natural transition orbital diagrams, a schematic of how the torsion angle is investigated, the energy, wavelength and oscillator strengths of the S_0 , S_1 - S_3 transitions for the S_0 minimised structures and the S_1 minimised structures.

VII. DEDICATION

LMH and PG would like to dedicate this work to several generations of strong women, who through their resilience have paved the way for LMH and PG to successfully pursue their journeys to become scientists of the modern world. There is much more inclusivity and respect than ever before. There is still much to do for the generations to come.

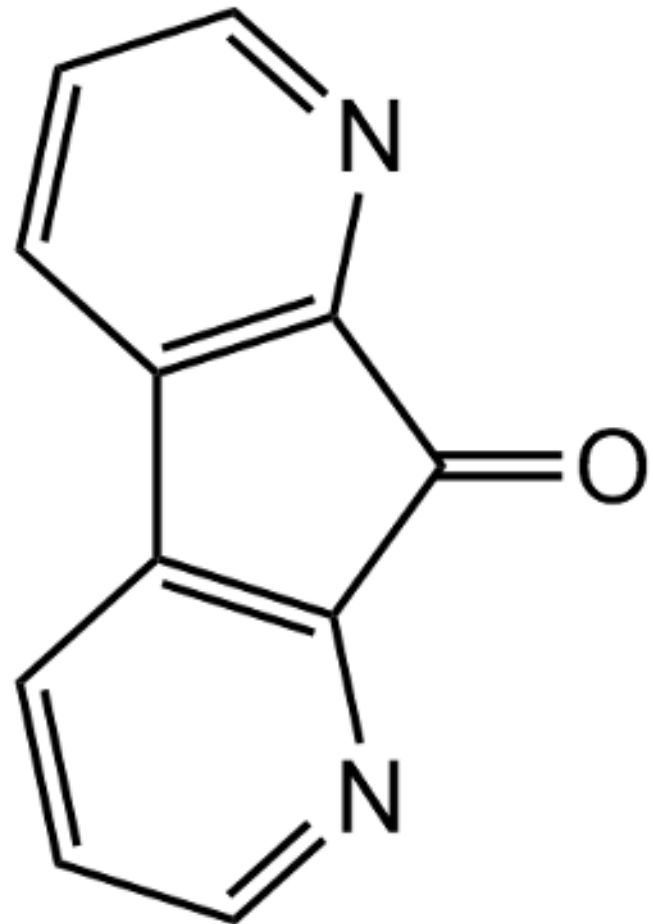
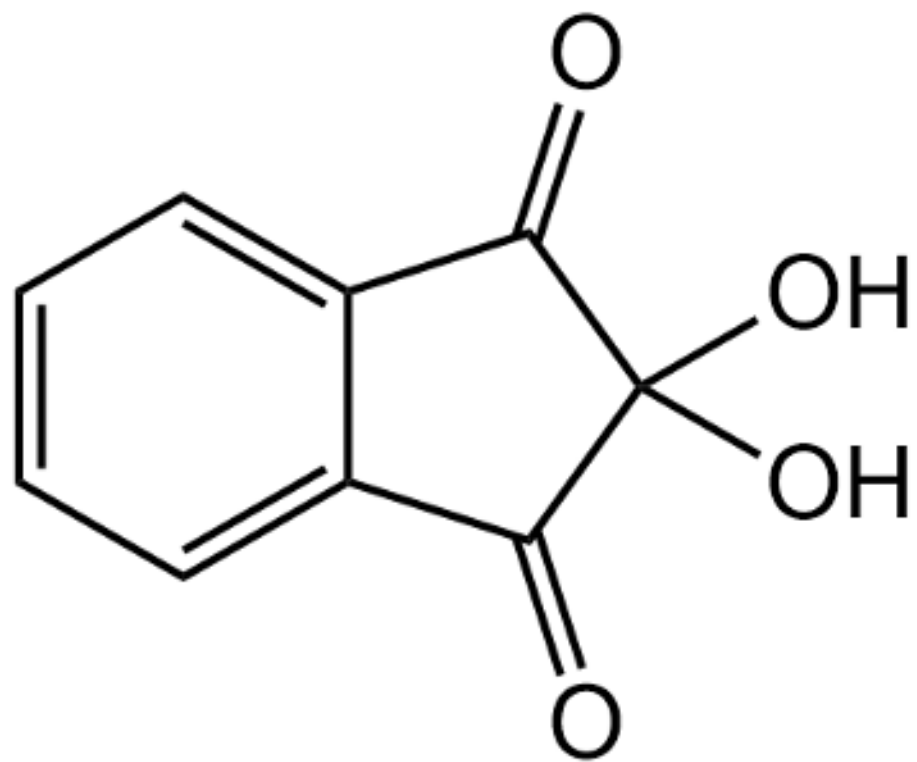
ACKNOWLEDGMENTS

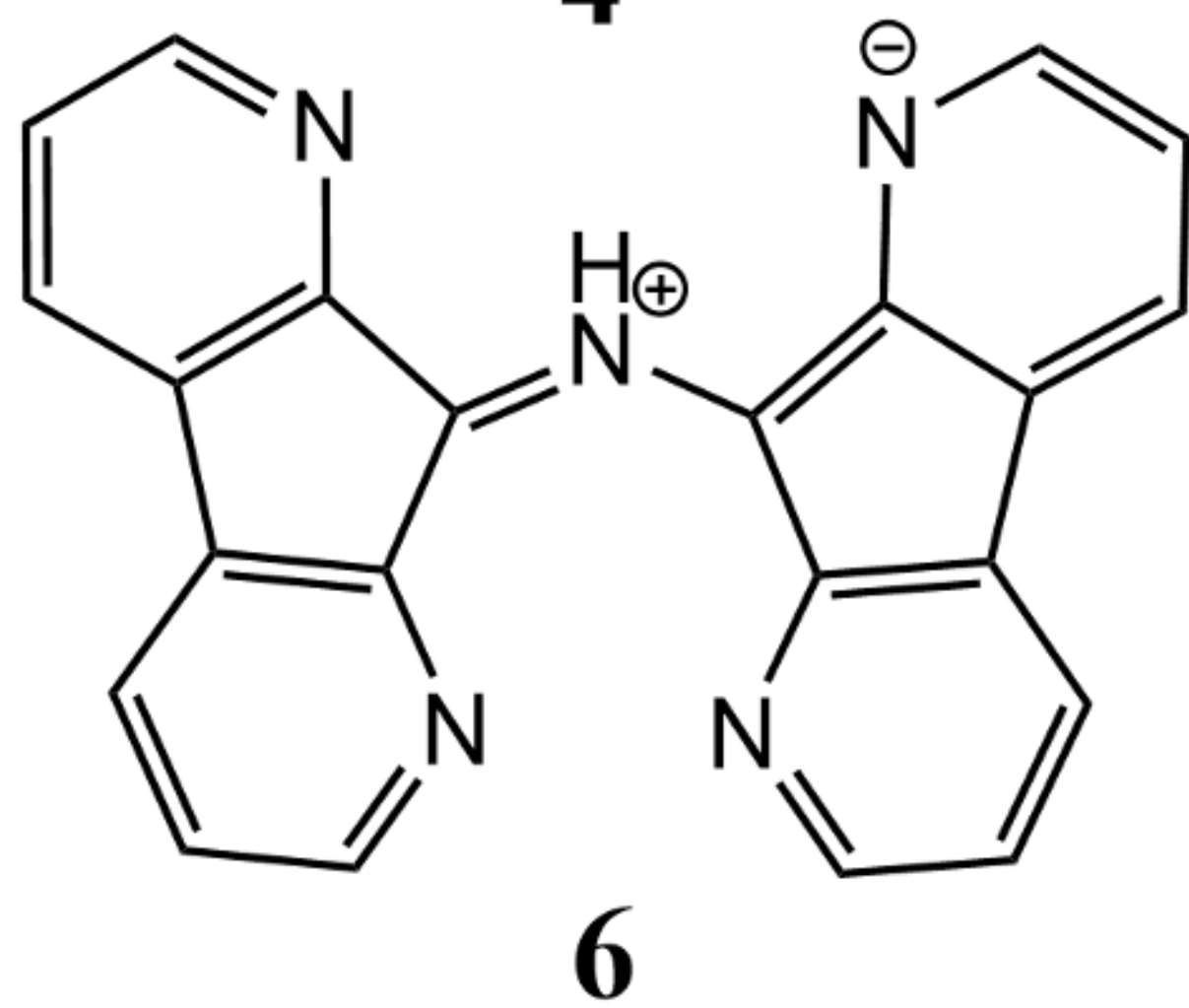
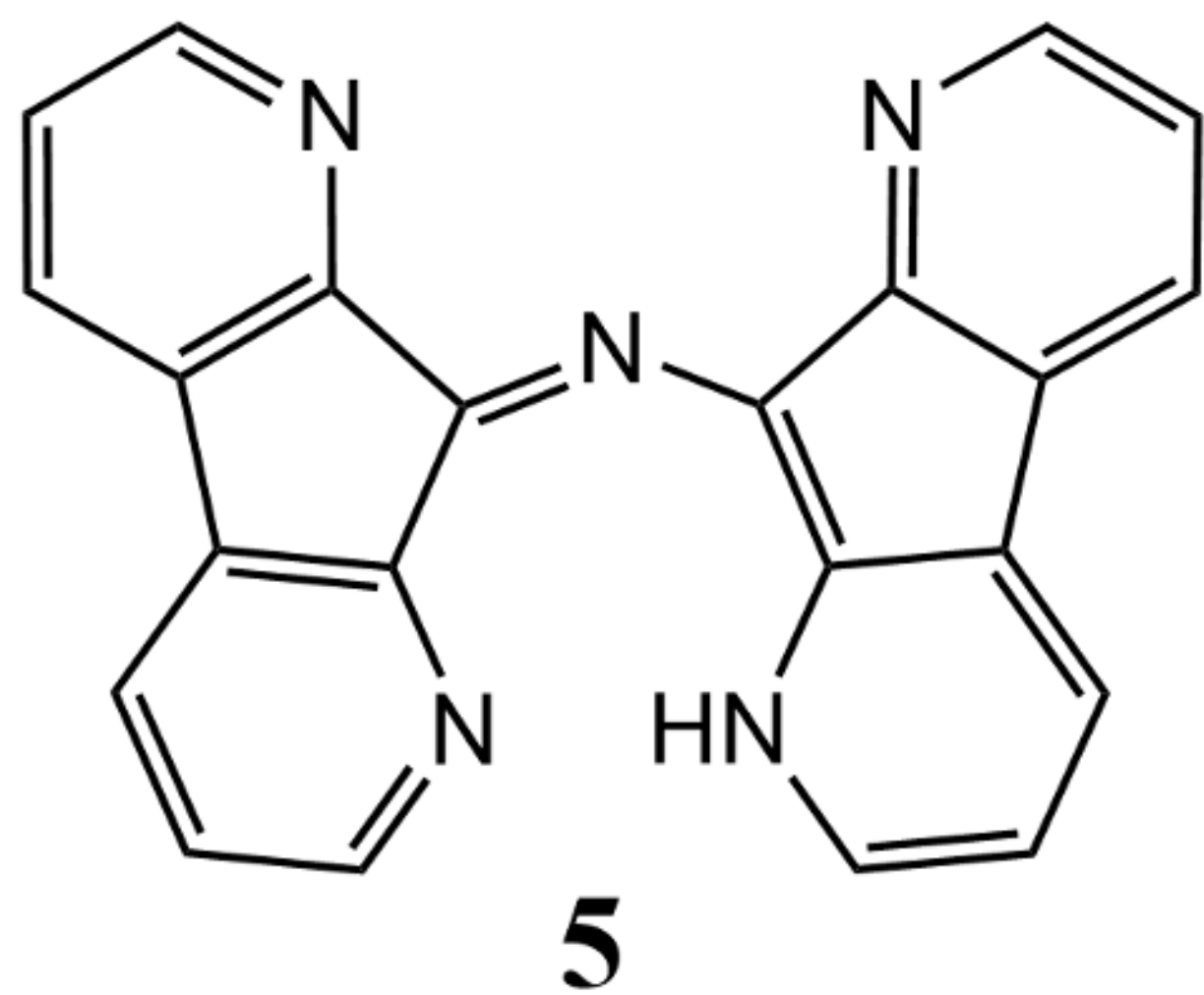
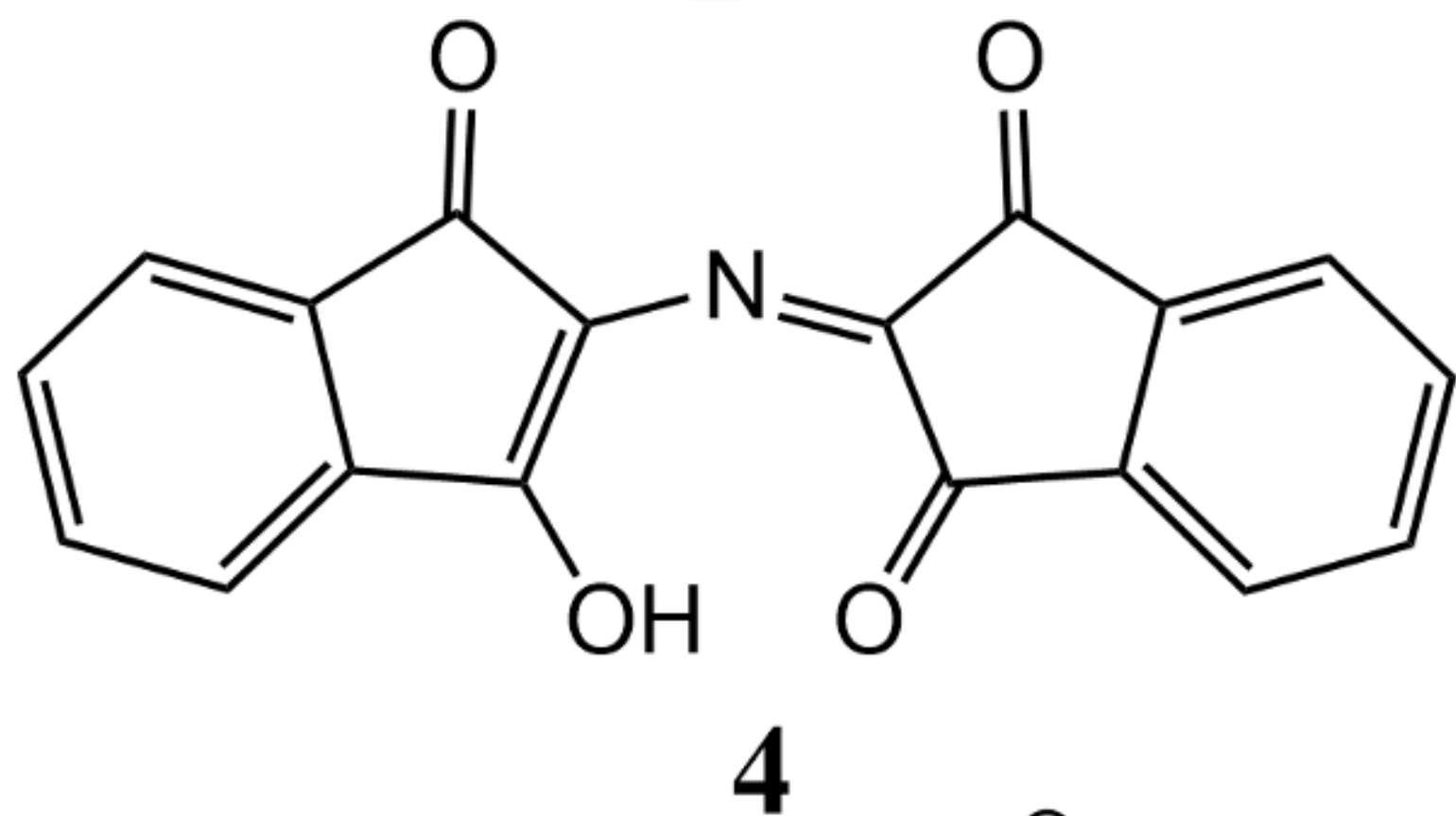
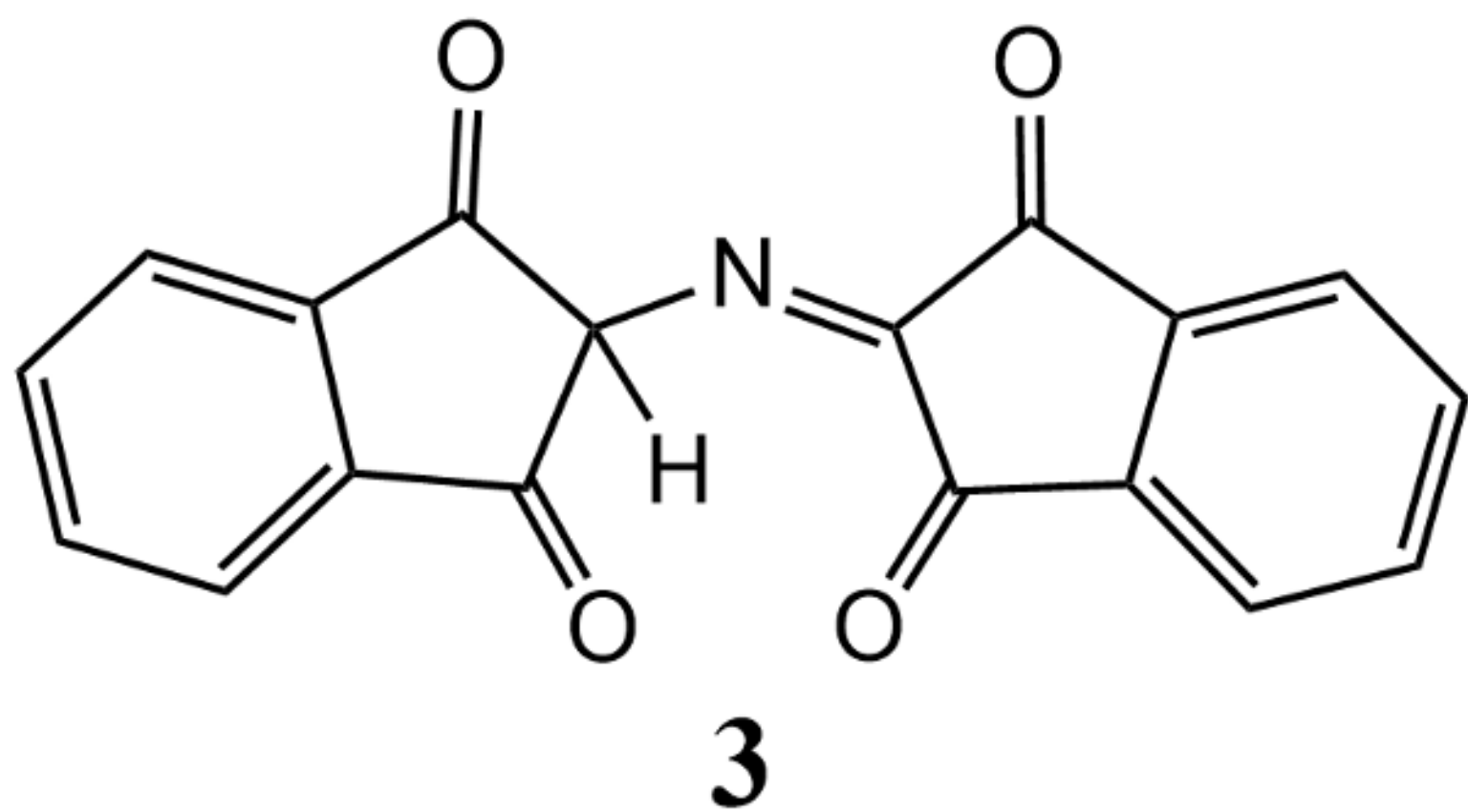
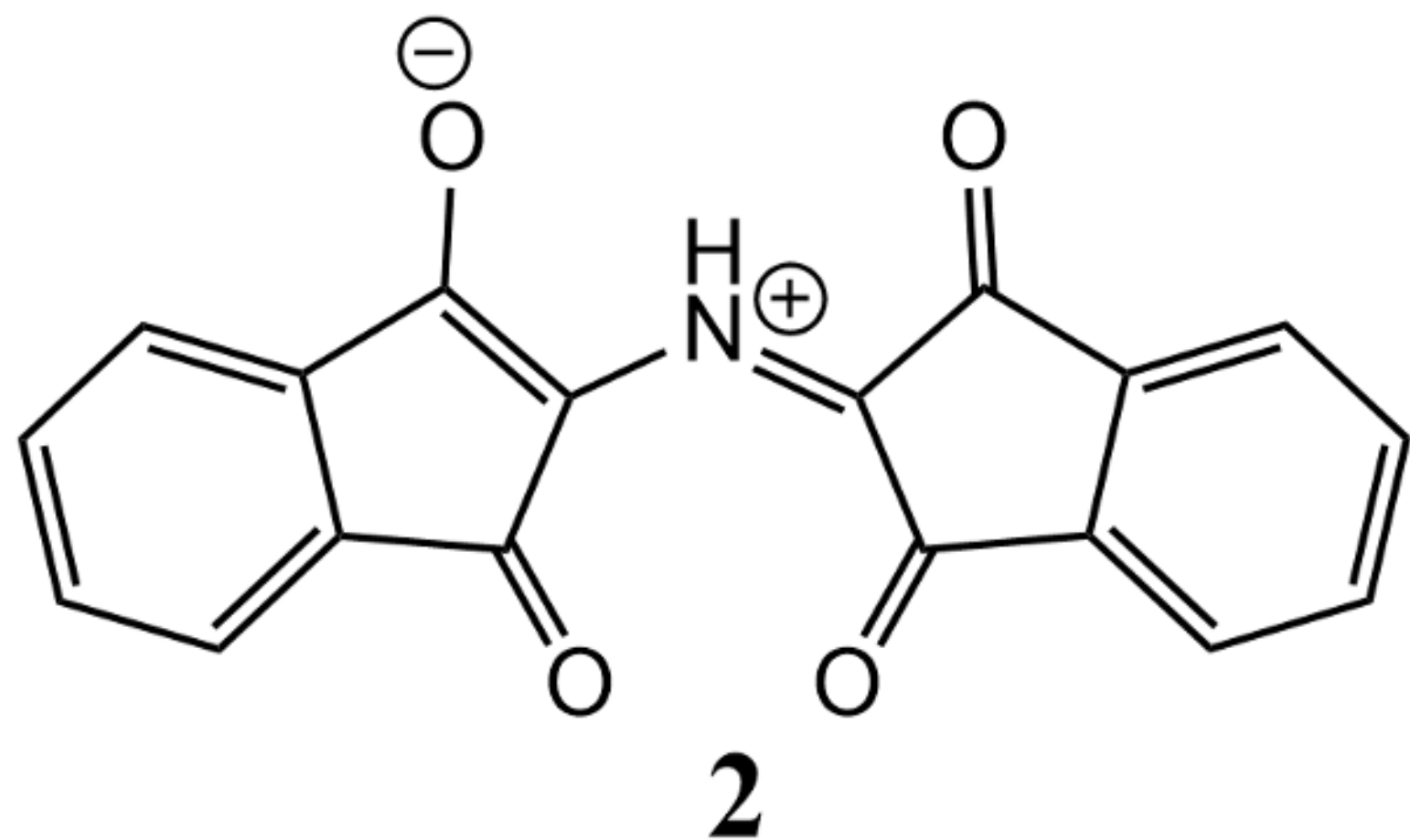
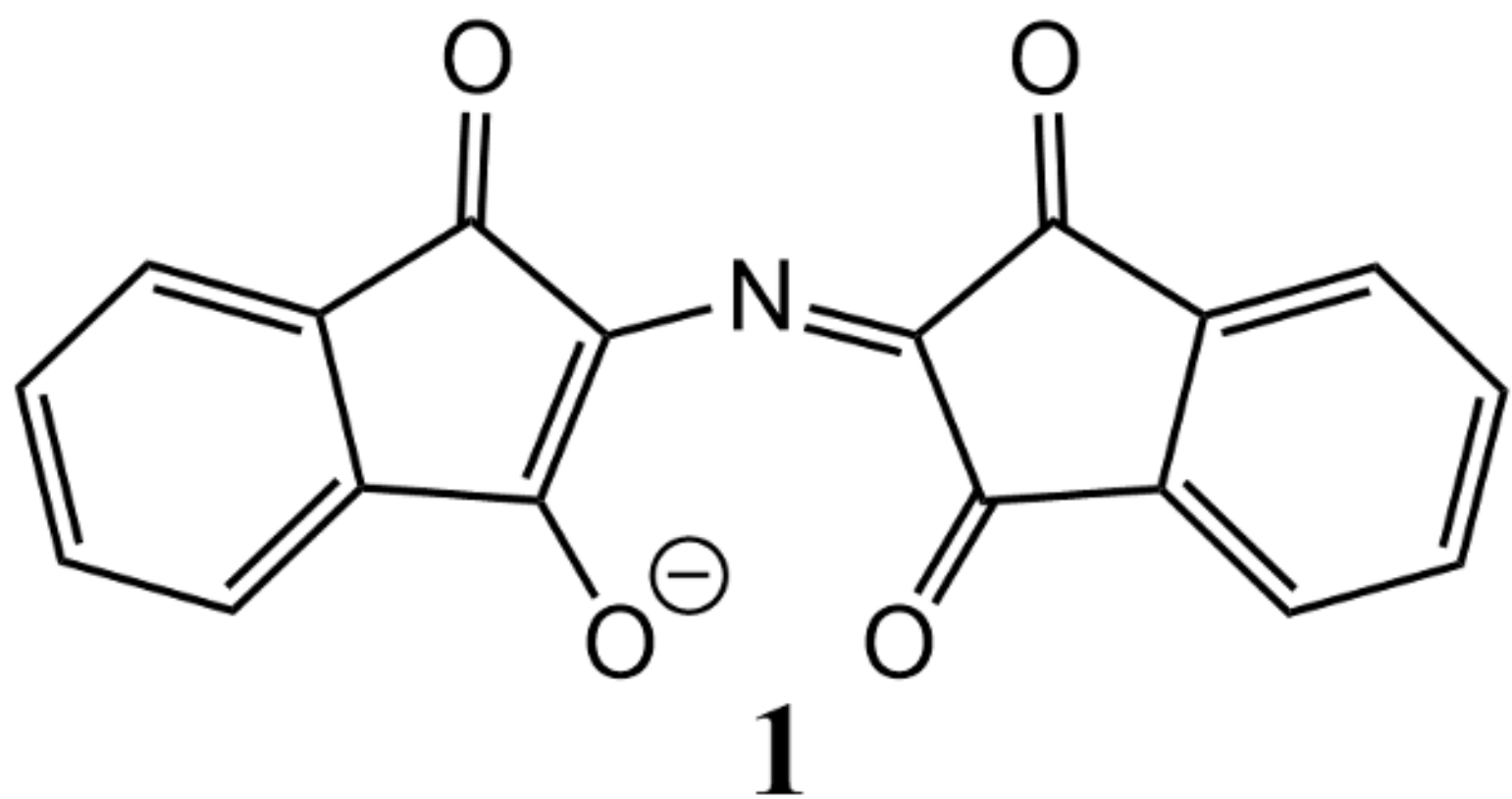
We wish to acknowledge the EPSRC Doctoral Training Partnership in conjunction with Loughborough University for funding LMH's PhD. The authors also recognise the use of the 'Hydra' High Performance System at Loughborough University. Finally, LMH and PG would like to thank the Defence Science and Technology Laboratory Staff (DSTL), Matthew Brooks and Helen Bandey for useful discussions.

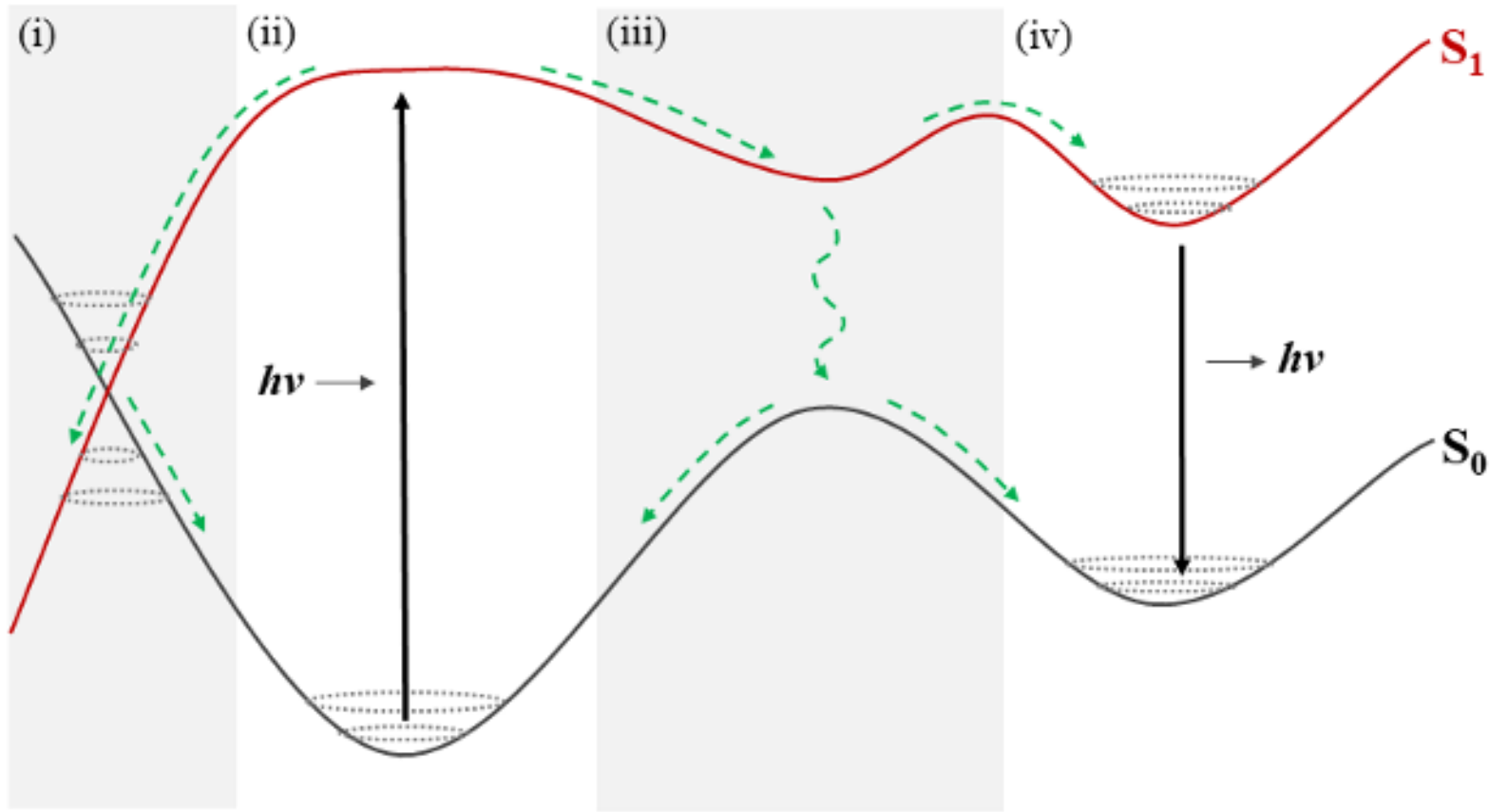
- ¹S. M. Bleay, R. S. Croxton, and M. De Puit, *Fingerprint Development Techniques* (Wiley Online Library, 2018).
- ²M. E. Casida and M. Huix-Rotllant, "Progress in time-dependent density-functional theory," *Annual review of physical chemistry* **63**, 287–323 (2012).
- ³S. Ghosh, P. Verma, C. J. Cramer, L. Gagliardi, and D. G. Truhlar, "Combining wave function methods with density functional theory for excited states," *Chemical reviews* **118**, 7249–7292 (2018).
- ⁴H. Lischka, D. Nachtigallova, A. J. Aquino, P. G. Szalay, F. Plasser, F. B. Machado, and M. Barbatti, "Multireference approaches for excited states of molecules," *Chemical reviews* **118**, 7293–7361 (2018).

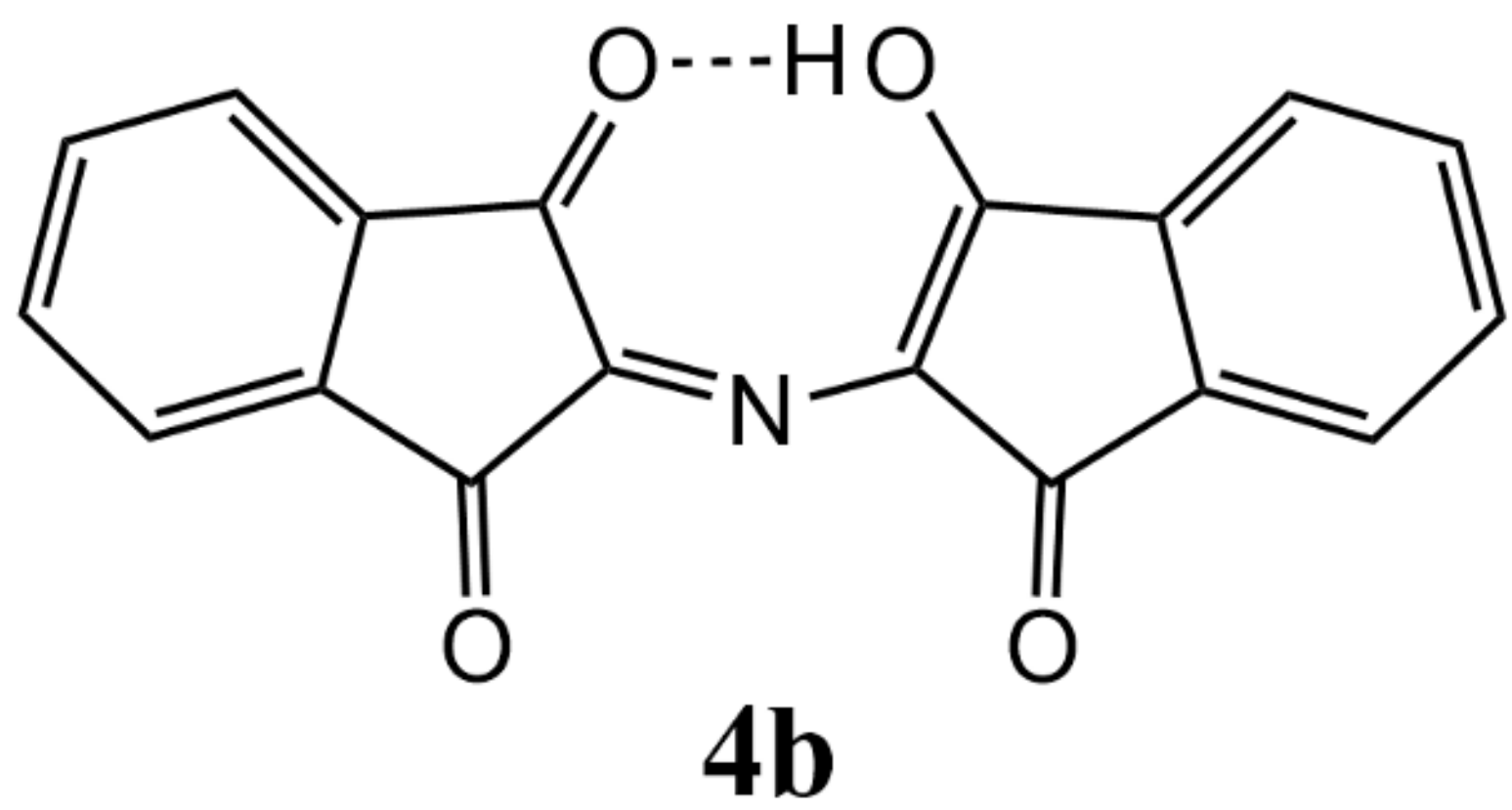
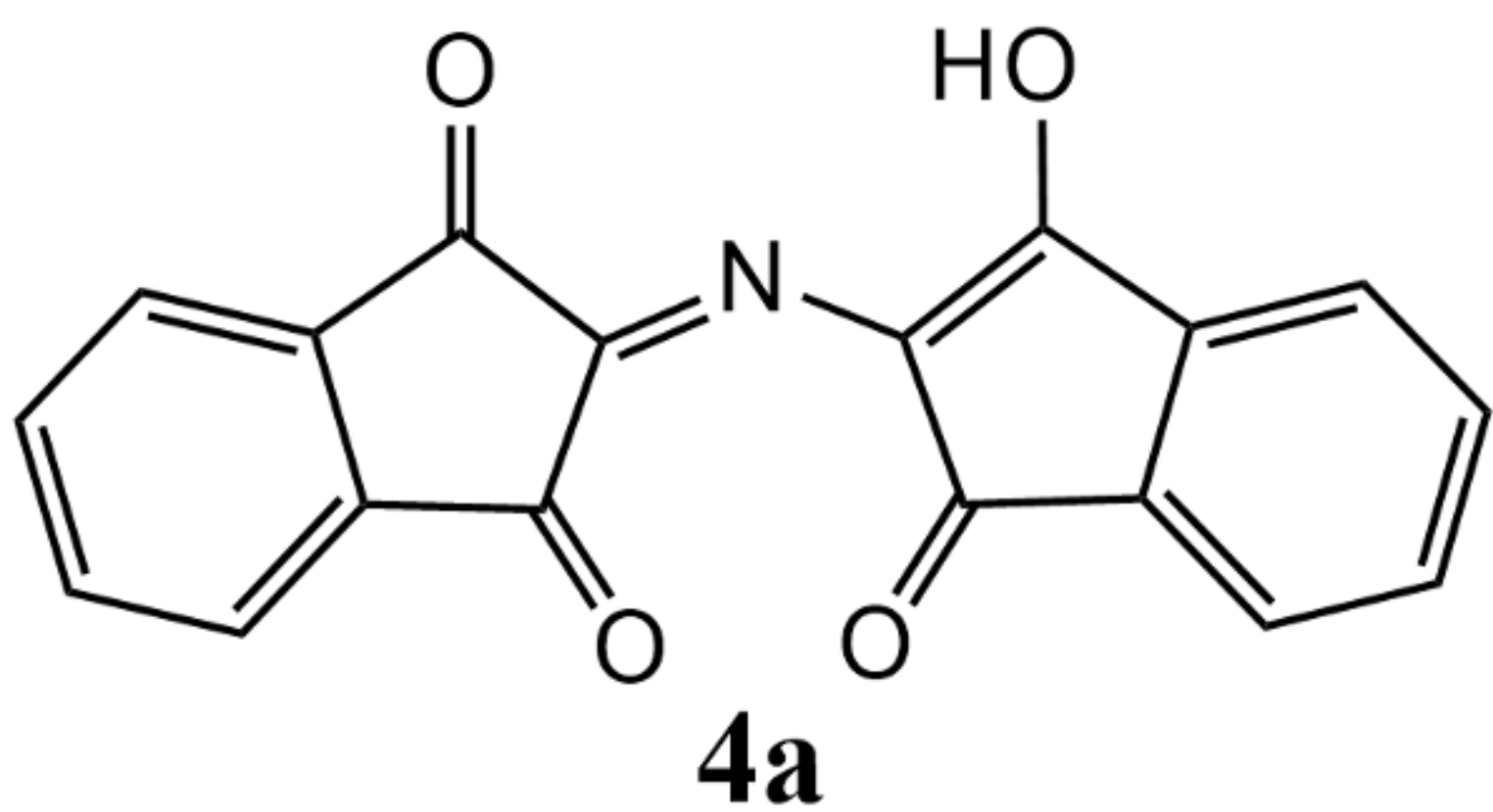
- ⁵S. Bleay, V. Sears, R. Downham, H. Bandey, A. Gibson, V. Bowman, L. Fitzgerald, T. Ciuksza, J. Ramadani, and C. Selway, "Fingerprint source book v2. 0," Home Office Centre for Applied Science and Technology (CAST), 665 (2017).
- ⁶S. Odén and B. Von Hofsten, "Detection of fingerprints by the ninhydrin reaction," *Nature* **173**, 449–450 (1954).
- ⁷A. Pounds, R. Grigg, and T. Mongkolaussavaratana, "The use of 1, 8-diazafluoren-9-one (dfo) for the fluorescent detection of latent fingerprints on paper: a preliminary evaluation," *Journal of Forensic Science* **35**, 169–175 (1990).
- ⁸D. Herod and E. Menzel, "Laser detection of latent fingerprints: ninhydrin followed by zinc chloride," *Journal of Forensic Science* **27**, 513–518 (1982).
- ⁹D. C. Wigfield, G. W. Buchanan, and S. M. Croteau, "On ruhemann's purple," *Canadian Journal of Chemistry* **58**, 201–205 (1980).
- ¹⁰R. Grigg, J. F. Malone, T. Mongkolaussavaratana, and S. Thianpatanagul, "Cycloaddition reaction relevant to the mechanism of the ninhydrin reaction. x-ray crystal structure of protonated ruhemann's purple, a stable 1, 3-dipole," *Journal of the Chemical Society, Chemical Communications*, 421–422 (1986).
- ¹¹F. Dietz, K. Rommel-Möhle, A. Schleitzer, and N. Tyutyulkov, "On the chromophore of the ninhydrin-amino acid color reaction," *Zeitschrift für Naturforschung B* **48**, 1133–1137 (1993).
- ¹²D. Wilkinson, "Study of the reaction mechanism of 1, 8-diazafluoren-9-one with the amino acid, l-alanine," *Forensic science international* **109**, 87–103 (2000).
- ¹³N. Nicolasora, R. Downham, L. Hussey, A. Luscombe, K. Mayse, and V. Sears, "A validation study of the 1, 2-indandione reagent for operational use in the uk: Part 1—formulation optimization," *Forensic science international* **292**, 242–253 (2018).
- ¹⁴N. Nicolasora, R. Downham, R.-M. Dyer, L. Hussey, A. Luscombe, and V. Sears, "A validation study of the 1, 2-indandione reagent for operational use in the uk: Part 2—optimization of processing conditions," *Forensic science international* **288**, 266–277 (2018).
- ¹⁵A. Luscombe and V. Sears, "A validation study of the 1, 2-indandione reagent for operational use in the uk: Part 3—laboratory comparison and pseudo-operational trials on porous items," *Forensic science international* **292**, 254–261 (2018).
- ¹⁶I. M. Alaoui, E. Menzel, M. Farag, K. Cheng, and R. Murdock, "Mass spectra and time-resolved fluorescence spectroscopy of the reaction product of glycine with 1, 2-indanedione in methanol," *Forensic science international* **152**, 215–219 (2005).
- ¹⁷X. Spindler, R. Shimmon, C. Roux, and C. Lennard, "The effect of zinc chloride, humidity and the substrate on the reaction of 1, 2-indanedione-zinc with amino acids in latent fingerprint secretions," *Forensic science international* **212**, 150–157 (2011).
- ¹⁸E. R. Menzel and J. Almog, "Latent fingerprint development by frequency-doubled neodymium: yttrium aluminum garnet (nd: Yag) laser: benzo (f) ninhydrin," *Journal of Forensic Science* **30**, 371–382 (1985).
- ¹⁹C. Lennard, P. Margot, M. Stoilovic, and R. Warrenner, "Synthesis of ninhydrin analogues and their application to fingerprint development: preliminary results," *Journal of the Forensic Science Society* **26**, 323–328 (1986).
- ²⁰J. Almog, A. Hirshfeld, A. Frank, H. Grant, Z. Harel, and Y. Ittah, "5-methylthio ninhydrin and related compounds: a novel class of fluorogenic fingerprint reagents," *Journal of Forensic Science* **37**, 688–694 (1992).
- ²¹R. R. Hark, D. B. Hauze, O. Petrovskaia, and M. M. Joullicé, "Synthetic studies of novel ninhydrin analogs," *Canadian journal of chemistry* **79**, 1632–1654 (2001).
- ²²N. D. Petraco, G. Proni, J. J. Jackiw, and A.-M. Sapse, "Amino acid alanine reactivity with the fingerprint reagent ninhydrin. a detailed ab initio computational study," *Journal of forensic sciences* **51**, 1267–1275 (2006).
- ²³D. Sapse and N. D. Petraco, "A step on the path in the discovery of new latent fingerprint development reagents: substituted ruhemann's purples and implications for the law," *Journal of Molecular Modeling* **13**, 943–948 (2007).
- ²⁴R. Elber, A. Frank, and J. Almog, "Chemical development of latent fingerprints: computational design of ninhydrin analogues," *Journal of Forensic Science* **45**, 757–760 (2000).
- ²⁵F. Bernardi, M. Olivucci, and M. Robb, "Modelling photochemical reactivity of organic systems—a new challenge to quantum computational

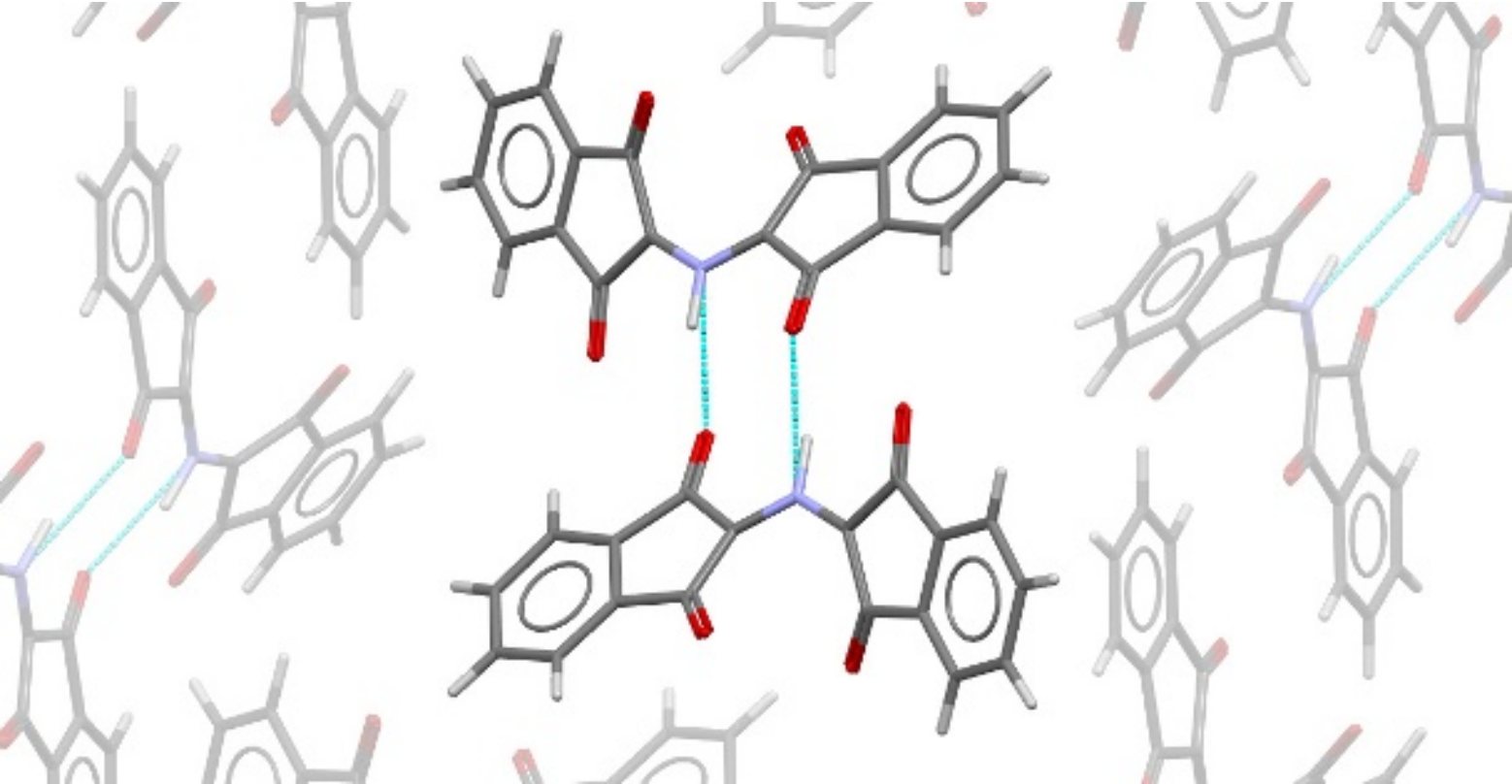
- chemistry," *Israel journal of chemistry* **33**, 265–276 (1993).
- ²⁶R. Crespo-Otero, Q. Li, and L. Blancafort, "Exploring potential energy surfaces for aggregation-induced emission—from solution to crystal," *Chemistry—An Asian Journal* **14**, 700–714 (2019).
- ²⁷M. Klessinger, "Conical intersections and the mechanism of singlet photoreactions," *Angewandte Chemie International Edition in English* **34**, 549–551 (1995).
- ²⁸Q. Li and L. Blancafort, "A conical intersection model to explain aggregation induced emission in diphenyl dibenzofulvene," *Chemical Communications* **49**, 5966–5968 (2013).
- ²⁹X.-L. Peng, S. Ruiz-Barragan, Z.-S. Li, Q.-S. Li, and L. Blancafort, "Restricted access to a conical intersection to explain aggregation induced emission in dimethyl tetraphenylsilole," *Journal of Materials Chemistry C* **4**, 2802–2810 (2016).
- ³⁰C. Lee, W. Yang, and R. G. Parr, "Development of the Colle-Salvetti correlation-energy formula into a functional of the electron density," *Phys. Rev. B* **37**, 785–789 (1988).
- ³¹A. D. Becke, "Density-functional thermochemistry. III. The role of exact exchange," *J. Chem. Phys.* **98**, 5648–5652 (1993).
- ³²T. Yanai, D. P. Tew, and N. C. Handy, "A new hybrid exchange–correlation functional using the coulomb-attenuating method (cam-b3lyp)," *Chemical physics letters* **393**, 51–57 (2004).
- ³³R. Ditchfield, W. J. Hehre, and J. A. Pople, "Self-consistent molecular-orbital methods. ix. an extended gaussian-type basis for molecular-orbital studies of organic molecules," *The Journal of Chemical Physics* **54**, 724–728 (1971).
- ³⁴P. C. Hariharan and J. A. Pople, "The influence of polarization functions on molecular orbital hydrogenation energies," *Theor. Chim. Acta* **28** (1973), 10.1007/bf00533485.
- ³⁵W. J. Hehre, R. Ditchfield, and J. A. Pople, "Self-consistent molecular orbital methods. xii. further extensions of gaussian-type basis sets for use in molecular orbital studies of organic molecules," *J. Chem. Phys.* **56** (1972), 10.1063/1.1677527.
- ³⁶A. Dreuw, J. L. Weisman, and M. Head-Gordon, "Long-range charge-transfer excited states in time-dependent density functional theory require non-local exchange," *J. Chem. Phys.* **119**, 2943–2946 (2003).
- ³⁷X. Li and M. J. Frisch, "Energy-represented direct inversion in the iterative subspace within a hybrid geometry optimization method," *Journal of chemical theory and computation* **2**, 835–839 (2006).
- ³⁸M. J. Frisch, G. W. Trucks, H. B. Schlegel, G. E. Scuseria, M. A. Robb, J. R. Cheeseman, G. Scalmani, V. Barone, G. A. Petersson, H. Nakatsuji, X. Li, M. Caricato, A. V. Marenich, J. Bloino, B. G. Janesko, R. Gomperts, B. Mennucci, H. P. Hratchian, J. V. Ortiz, A. F. Izmaylov, J. L. Sonnenberg, D. Williams-Young, F. Ding, F. Lipparini, F. Egidi, J. Goings, B. Peng, A. Petrone, T. Henderson, D. Ranasinghe, V. G. Zakrzewski, J. Gao, N. Rega, G. Zheng, W. Liang, M. Hada, M. Ehara, K. Toyota, R. Fukuda, J. Hasegawa, M. Ishida, T. Nakajima, Y. Honda, O. Kitao, H. Nakai, T. Vreven, K. Throssell, J. A. Montgomery, Jr., J. E. Peralta, F. Ogliaro, M. J. Bearpark, J. J. Heyd, E. N. Brothers, K. N. Kudin, V. N. Staroverov, T. A. Keith, R. Kobayashi, J. Normand, K. Raghavachari, A. P. Rendell, J. C. Burant, S. S. Iyengar, J. Tomasi, M. Cossi, J. M. Millam, M. Klene, C. Adamo, R. Cammi, J. W. Ochterski, R. L. Martin, K. Morokuma, O. Farkas, J. B. Foresman, and D. J. Fox, "Gaussian-09 Revision E.01," (2016), gaussian Inc. Wallingford CT.
- ³⁹R. L. Martin, "Natural transition orbitals," *J. Chem. Phys.* **118**, 4775–4777 (2003).
- ⁴⁰R. Dennington, T. Keith, and J. Millam, "Gaussview 5.0, gaussian," Inc, Wallingford (2008).
- ⁴¹C. R. Groom, I. J. Bruno, M. P. Lightfoot, and S. C. Ward, "The cambridge structural database," *Acta Crystallographica Section B: Structural Science, Crystal Engineering and Materials* **72**, 171–179 (2016).
- ⁴²C. F. Macrae, I. J. Bruno, J. A. Chisholm, P. R. Edgington, P. McCabe, E. Pidcock, L. Rodriguez-Monge, R. Taylor, J. Streek, and P. A. Wood, "Mercury csd 2.0—new features for the visualization and investigation of crystal structures," *Journal of Applied Crystallography* **41**, 466–470 (2008).
- ⁴³S. Bai, R. Mansour, L. Stojanović, J. M. Toldo, and M. Barbatti, "On the origin of the shift between vertical excitation and band maximum in molecular photoabsorption," *Journal of molecular modeling* **26**, 1–9 (2020).



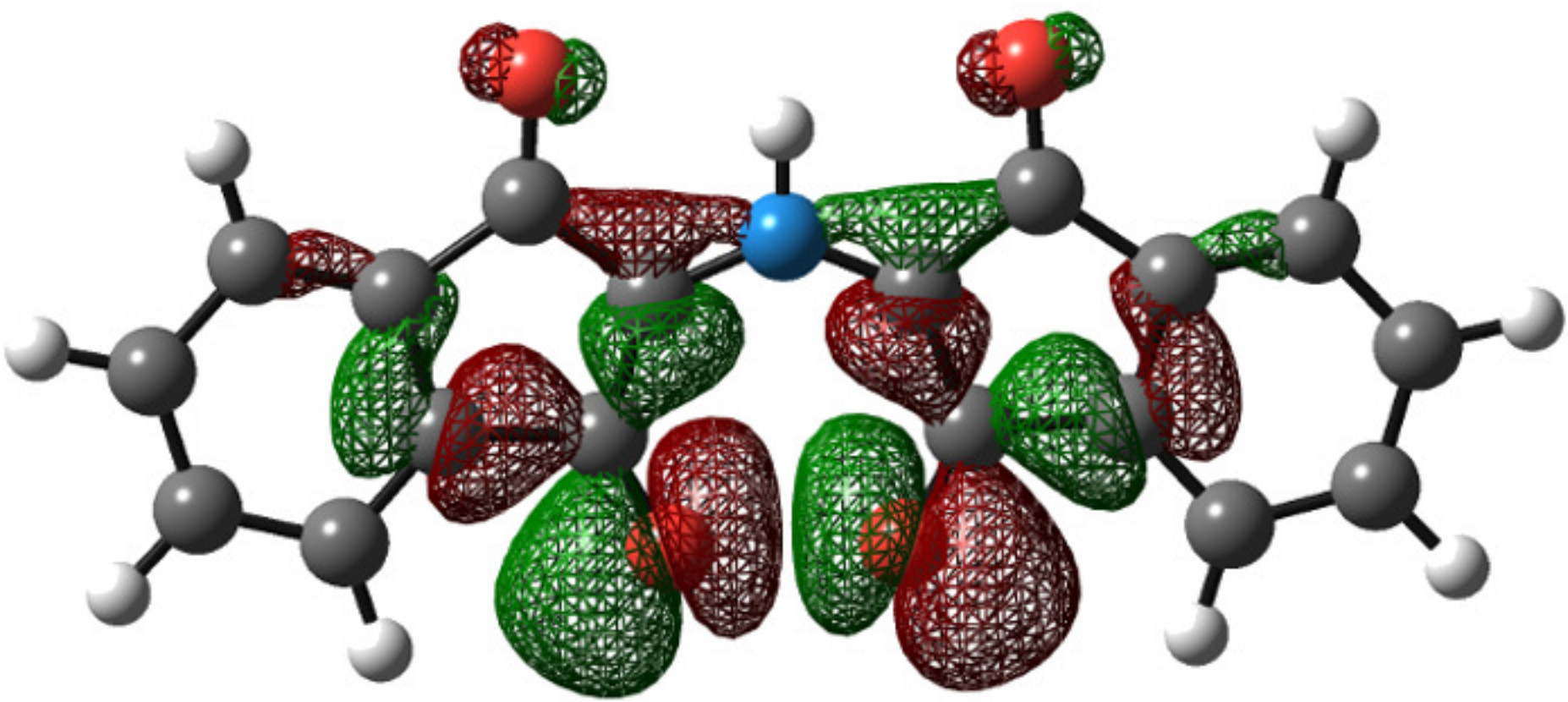






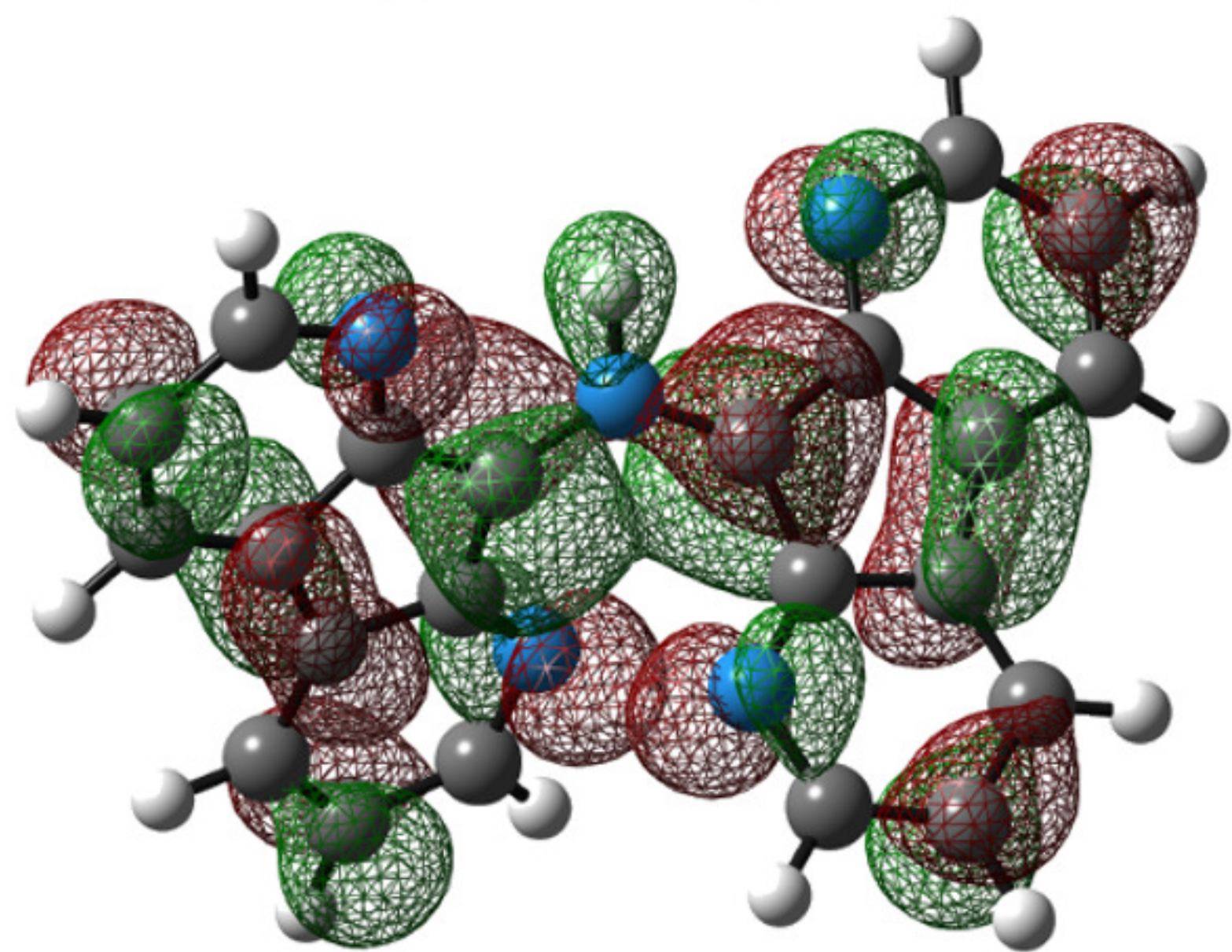
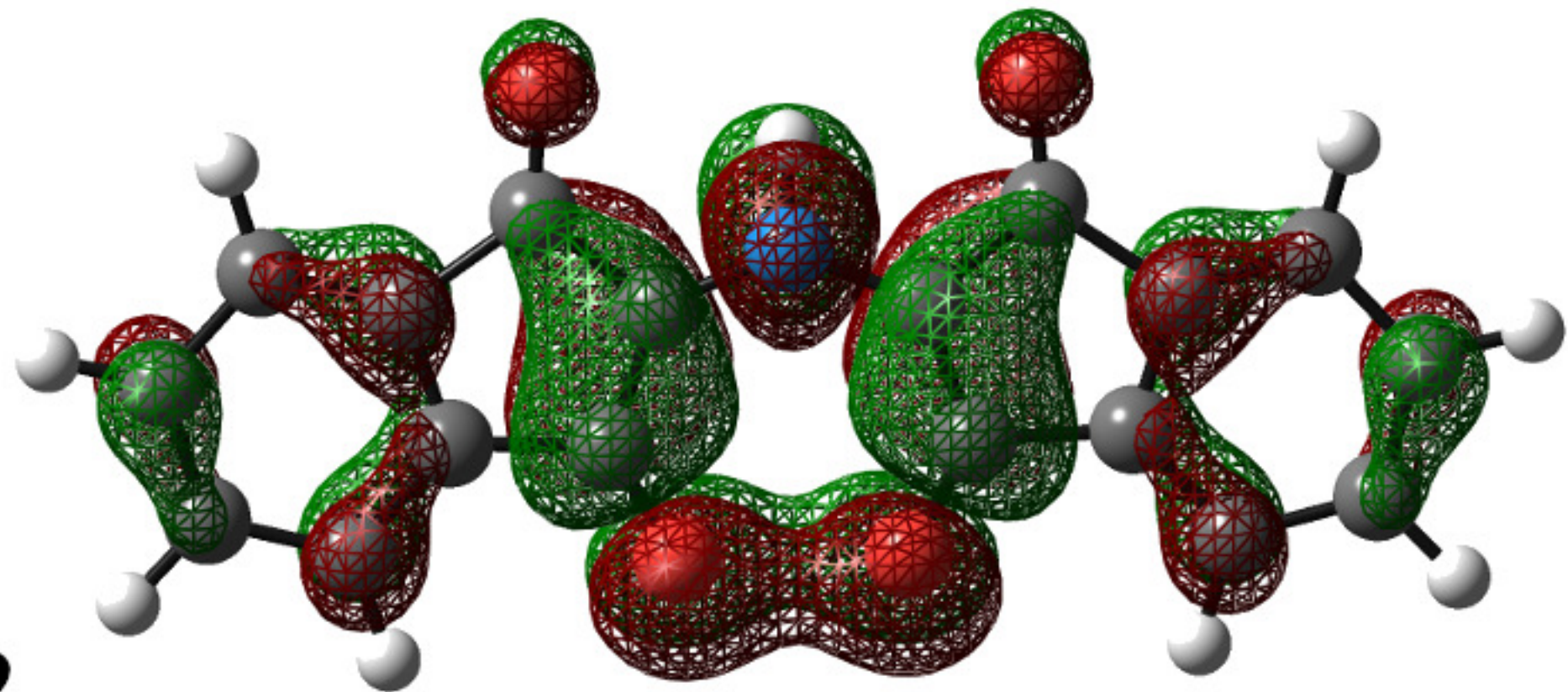


Hole



2

Electron



6

